Coherent Structures and Extreme Events in Rotating Multiphase Turbulent Flows

L. Biferale, F. Bonaccorso, and I. M. Mazzitelli
Department of Physics and INFN, University of Rome Tor Vergata, Via della Ricerca Scientifica 1, 00133 Rome, Italy

M. A. T. van Hinsberg
Department of Physics, Eindhoven University of Technology, 5600 MB Eindhoven, The Netherlands

A. S. Lanotte
CNR-ISAC and INFN, Strada Provinciale Lecce-Monteroni, 73100 Lecce, Italy

S. Musacchio
Université de Nice Sophia Antipolis, CNRS, Laboratoire J. A. Dieudonné, UMR 7351, 06100 Nice, France

P. Perlekar
TIFR Centre for Interdisciplinary Sciences, 21 Brundavan Colony, Narsingi, Hyderabad 500075, India

F. Toschi
Department of Physics, Eindhoven University of Technology, 5600 MB Eindhoven, The Netherlands and IAC CNR, Via dei Taurini 19, 00185 Roma, Italy

(Received 2 April 2016; revised manuscript received 2 July 2016; published 21 November 2016)

By using direct numerical simulations (DNS) at unprecedented resolution, we study turbulence under rotation in the presence of simultaneous direct and inverse cascades. The accumulation of energy at large scale leads to the formation of vertical coherent regions with high vorticity oriented along the rotation axis. By seeding the flow with millions of inertial particles, we quantify—for the first time—the effects of those coherent vertical structures on the preferential concentration of light and heavy particles. Furthermore, we quantitatively show that extreme fluctuations, leading to deviations from a normal-distributed statistics, result from the entangled interaction of the vertical structures with the turbulent background. Finally, we present the first-ever measurement of the relative importance between Stokes drag, Coriolis force, and centripetal force along the trajectories of inertial particles. We discover that vortical coherent structures lead to unexpected diffusion properties for heavy and light particles in the directions parallel and perpendicular to the rotation axis.

DOI: 10.1103/PhysRevX.6.041036

Subject Areas: Fluid Dynamics, Geophysics, Particles and Fields

I. INTRODUCTION

The dynamics of fluids under strong rotation is a challenging problem in the field of hydrodynamics and magnetohydrodynamics [1,2], with key applications to geophysical and astrophysical problems (oceans, Earth's atmosphere and inner mantle, gaseous planets, planetesimal formations) and engineering (turbomachinery, chemical mixers) [3–8]. A considerable number of experiments [9–22] have been devoted to investigating how turbulence is affected by rotation (for a recent review of experimental and numerical results, see Ref. [23]). The strength of rotation is measured by the Rossby number $\mathrm{Ro} = (\epsilon_f k_f^2)^{1/3}/\Omega$, defined as the ratio of the rotation time, $\tau_\Omega = 1/\Omega$, and the flow time scale, $\epsilon_f k_f^2$. Here, ϵ_f and k_f are the input of energy and the wave number where the external forcing is applied (see Table I). The most striking phenomenon originated by the Coriolis force is the formation of intense and coherent columnar vortical structures (see Fig. 1), which has been observed in numerical simulations [15–19] and in experiments for rotating turbulence produced by an oscillating grid [9], for decaying turbulence [10–12], forced turbulence [14], and turbulent convection [24]. The appearance of these large-scale vortices is associated to a noticeable two dimensionalization of the flow in the plane perpendicular to the rotation axis. Rotating turbulent dynamics with Rossby number $O(1)$ is typical of many industrial and geophysical applications, but key fundamental questions are still open. These are mostly connected to the nature of the interaction between the two-dimensional vortical structures and the underlying fully three-dimensional anisotropic turbulent fluctuations, and to the way this impacts the Lagrangian dynamics of particles dispersed in the flow. In this paper, we

TABLE I. Eulerian dynamics parameters. N, number of collocation points per spatial direction; Ω, rotation rate; k_Ω, the Zeman wave number; ν, kinematic viscosity; $\epsilon = \nu \int d^3x \sum_{ij} (\nabla_i u_j)^2$, viscous energy dissipation; $\epsilon_f = \int d^3x \sum_i f_i u_i$, energy injection; $u_0^2 = 1/3 \int d^3x \sum_i u_i^2$; $\eta = (\nu^3/\epsilon)^{1/4}$, Kolmogorov dissipative scale; $dx = L_0/N$, numerical grid spacing; $L_0 = 2\pi$, box size; $\tau_\eta = (\nu/\epsilon)^{1/2}$, Kolmogorov dissipative time; $\mathrm{Re}_\lambda = (u_0\lambda)/\nu$, Reynolds number based on the Taylor microscale; $\lambda = (15\nu u_0^2/\epsilon)^{1/2}$, Taylor microscale; $\mathrm{Ro} = (\epsilon_f k_f^2)^{1/3}/\Omega$, Rossby number defined in terms of the energy injection properties, where $k_f = 5$ is the wave number where the forcing is acting; f_0, intensity of the Ornstein-Uhlenbeck forcing; τ_f, decorrelation time of the forcing; $T_0 = u_0/L_0$, Eulerian large-scale eddy turnover time; α, coefficient of the damping term $\alpha\Delta^{-1}\boldsymbol{u}$. The typical total duration for a production run at resolution $N = 2048$ is $T_{\mathrm{tot}} = 20$.

N	Ω	k_Ω	ν	ϵ	ϵ_f	u_0^2	η/dx	τ_η/dt	Re_λ	Ro	f_0	τ_f	T_0	α
1024	4	7	7×10^{-4}	1.2	1.2	1.05	0.67	120	150	0.78	0.02	0.023	0.17	0.0
1024	10	48	6×10^{-4}	0.46	0.59	1.6	0.76	294	580	0.24	0.02	0.023	0.25	0.1
2048	4	7	2.8×10^{-4}	1.2	1.2	1.05	0.67	380	230	0.76	0.02	0.023	0.17	0.0
2048	10	48	2.2×10^{-4}	0.45	0.64	1.7	0.72	550	1170	0.25	0.02	0.023	0.3	0.1
4096	10	49	1×10^{-4}	0.46	0.65	1.7	0.78	1010	1600	0.25	0.02	0.023	0.3	0.1

empirically assess the Eulerian and Lagrangian statistical properties of rotating flow by using high-resolution direct numerical simulations at unprecedented resolution. We present the first simultaneous study of Lagrangian and Eulerian properties, seeding the strongly rotating flow with billions of small particles with and without inertia. In particular, we investigate statistical events much larger than the root-mean-squared fluctuations, measuring high-order moments of velocity increments both along the rotation axis and in the perpendicular plane. To disentangle the statistical properties of the 2D structures from the underlying 3D turbulent background, we propose to decompose the velocity field on its instantaneous mean profile, obtained by averaging along the rotation axis, and on the fluctuations around it. We show that there exits a highly nontrivial entanglement among the vortical structures and the 3D background leading to a complex non-Gaussian distribution for both 2D and 3D components. Similarly, we quantify the singular role played by vortical structures for the preferential concentration of inertial particles' trajectories. We assess for the first time the properties of inertia in driving light and heavy particles advected by the rotating flow assessing the relative importance of the centrifugal, Coriolis, added-mass, and Stokes forces, and we show that rotation is extremely efficient in separating heavy from light particles, defeating the mixing properties of the underlying turbulent flow.

A. Eulerian fields

Rotation causes the generation of inertial waves in the flow [1]. Waves, and the associated instabilities, are of general interest given their fundamental character in atmospheric and oceanographic applications. The interplay between inertial waves and the two-dimensional three-components (2D3C) turbulent structures that develop in rotating turbulent flows is the subject of active debate. Several authors [16,25–29] have discussed the possibility of describing the dynamics of rapidly rotating 3D flows (limit of Rossby number much smaller than 1), in terms of wave turbulence triggered by triadic resonant interactions (for reviews on wave turbulence, see Refs. [30–32]). At the same time, experimental [13,33] and numerical studies [20,21] indicate that 2D turbulence provides an effective description of many aspects of rotating flows (for a recent review on 2D turbulence, see Ref. [34]).

Theoretical studies [26,27], addressing inertial wave turbulence theory with a complete numerical solution in addition to the results of quasinormal closures, and numerical simulations [16] have shown that the nonlinear wave interactions tend to concentrate energy in the wave plane normal to the rotation axis, favoring the transfer of energy from the 3D fast modes toward the 2D slow manifold (see also Ref. [25] for a generalized quasinormal approach, not restricted to the asymptotic limit and with quantitative comparisons to direct numerical simulation data). This has been proposed as a mechanism that creates the columnar vortices [23]. In particular, triadic wave interactions are able to capture the main part of the so-called "spectral buffer layer," i.e., the spectral region close to the 2D slow manifold [27]. On the other hand, the leading resonant three-wave interactions cannot transfer energy directly to the 2D modes [16,20] and the wave approximation cannot be uniform as a function of the wave number. In other words, the wave turbulence description ceases to be valid for very small wave numbers in the direction of the rotation axis, $k_{||} = \boldsymbol{k} \cdot \Omega/\Omega \simeq 0$, and for very large wave numbers in the perpendicular direction, $k_\perp = \boldsymbol{k} - \boldsymbol{k} \cdot \Omega/\Omega$ [29]; see also Ref. [26] for a discussion about the decoupling of the 2D manifold. In such spectral regions the coupling of modes by near-resonant and nonresonant triads has been numerically investigated at moderate Rossby numbers in Ref. [35]. Previously, the decoupling of the 2D slow mode was questioned in Ref. [26], while a theoretical work [36] based on stability analysis of the 2D flow has shown the existence of a critical Rossby number below which 3D rotating flow becomes exactly 2D in the long-time limit.

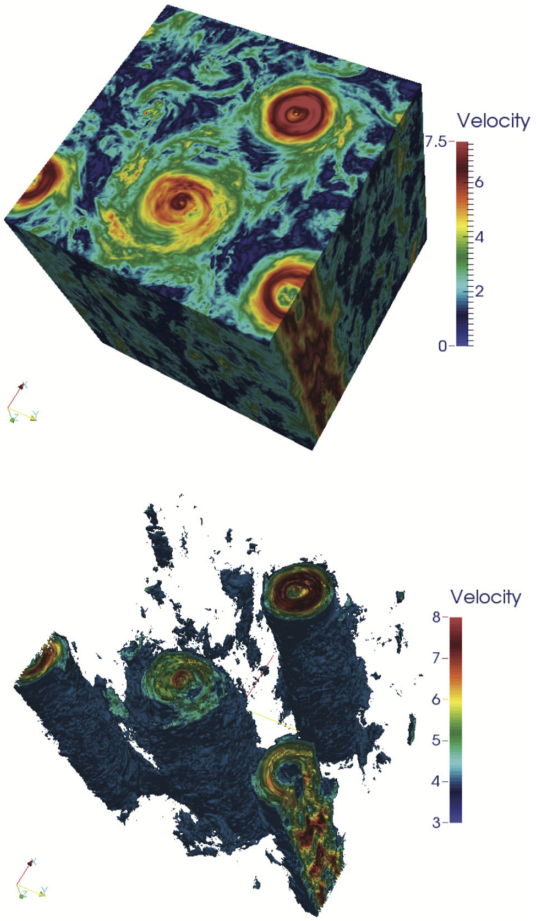

FIG. 1. Top: 3D rendering of a turbulent flow at Rossby number $\mathrm{Ro} = 0.25$ and rotation rate $\Omega = 10$. An inverse energy cascade is present in the turbulent dynamics. The stationary behavior is characterized by the formation of three cyclonic coherent columnar vortices emerging from the background of 3D turbulent fluctuations. Bottom: Vortical structures parallel to the rotation axis. Note the turbulent fluctuations exist also inside the core of each vortex. Color scale is based on the velocity amplitude.

The scenario is complicated by the fact that the predictions obtained from the wave turbulence in infinite domains, with a continuous wave number space, could differ from the observations of numerical simulations and experiments, which necessarily deal with fluids confined in finite volumes. Note, in particular, that the exact decoupling of the 2D slow manifold from the inertial waves, due to resonant three-wave interactions, is not proven in the continuous case (see Ref. [26]). The discretization of the wave numbers in finite volumes causes a gap between the 2D manifold and the 3D modes that could favor the decoupling of the 2D dynamics (see Ref. [16] and references therein). The wave turbulence theory has been recently applied to the case of an infinite fluid layer confined between two solid boundaries [28]. In this case, the discretization of the $k_{||}$ allows us to address the dynamics of the 2D manifold and its relationship with the wave modes. In particular, it has been shown that the presence of a strong 2D mode might have a strong feedback on the waves dynamics, as inertial waves can be scattered by the vortices [28]. Along this line, recent experiments [37] and numerical simulations [38] have shown that a significant fraction of the kinetic energy is concentrated in the inertial waves whose period is shorter than the turnover time of the 2D structures, while waves with longer period are scrambled by the turbulent advection. Finally, recent numerical investigation of the rotating Taylor-Green flow [22] has shown that the limits of small Rossby and large Reynolds numbers do not commute, and could lead to different asymptotic regimes, displaying either the wave turbulence or the quasi-2D inverse cascade. As a result, the combined information from theory, numerics, and experiments is still far from being sufficient to make a clear picture of the rotating turbulence. It is safe to say that we do not control the physics of rotating turbulence for realistic setup, in the presence of confinement, with external forcing and at Rossby number $O(1)$, concerning both mean spectral quantities and fluctuations on top of them.

B. Lagrangian particles

Lagrangian dynamics in rotating flows is at the core of many different physical and engineering problems, ranging from the dispersion and diffusion of pollutants, living species, or mixing of chemical reagents, to cite just a few examples. However, the bulk of knowledge collected about the Eulerian properties of the flow has no counterpart in the Lagrangian framework. In the past decade, a significant advance in the understanding of the dynamics of inertial particles suspended in turbulent flows has been achieved, notably for homogeneous and isotropic flows [39]. In the specific framework of particle dynamics in rotating flows, very few results are available. We mention a theoretical prediction for the spatial distribution of small, heavy particles in rotating turbulence [40], a prediction for the dispersion of fluid tracers in rotating turbulence [41], and the experimental study of the tracerlike particles acceleration statistics [42].

In this paper, we present the first attempt to assess the importance of Coriolis and centrifugal forces on the dynamical evolution and spatial dispersion of light and heavy particles, within the point-particles approximation. We show that the combined effect of inertia plus rotation leads to a singular behavior for the particles' statistics. In particular, the preferential sampling of high or low vorticity regions is strongly enhanced and characterized by anisotropic contributions on opposite directions: light particles tend to diffuse mainly vertically (i.e., along the rotation axis) while heavy particles are strongly confined in horizontal planes (see Fig. 2). As a result, the relative importance of Coriolis, centrifugal, or added-mass forces might vary by orders of magnitude comparing light or heavy families. We suggest that, at any rotation rate of practical interest, both the 2D and the 3D turbulent

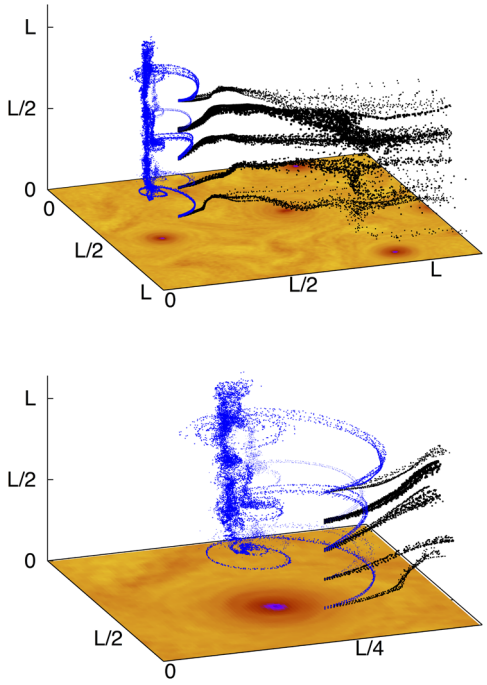

FIG. 2. 3D rendering of the evolution of two different puffs of particles, one light (blue) and one heavy (black), released in a turbulent flow at Rossby number Ro = 0.25. Particles are injected on the same rotation axis and with a velocity equal to that of the underlying fluid. The dispersion dynamics follows two different evolutions: light particles get trapped by the nearest columnar vortex and diffuse mainly vertically, while heavy particles tend to avoid the columnar structures and diffuse mainly horizontally. In the bottom plane, we show the intensity of the vertical vorticity averaged along the rotation axis. Bottom panel shows an enlargement of the top panel close to one intense vertical structure.

structures are coupled together and that any attempt to separate them into a weak wave turbulence coupled with a quasi-2D slow dynamics in the plane perpendicular to the rotation axis might fail to capture key properties for both Eulerian and Lagrangian statistics. This is an important remark for the phenomenology of Eulerian and Lagrangian rotating turbulence and to further improve its modelization.

This paper is organized as follows. In Sec. II, we discuss the numerical setup concerning both Eulerian and Lagrangian properties. In Sec. III, we discuss the Eulerian statistical properties at changing both Rossby and Reynolds numbers, while in Sec. IV, we present the main results concerning the dispersion of light or heavy particles. Our conclusions follow in Sec. V.

II. NUMERICAL METHODS

A. Equation of motion for the Eulerian flow and for the Lagrangian trajectories

The dynamics of an incompressible velocity field $\boldsymbol{u}$ in a rotating reference frame with angular frequency Ω is given by the three-dimensional Navier-Stokes equations (NSE):

$$\frac{\partial \boldsymbol{u}}{\partial t} + \boldsymbol{u}\cdot\nabla\boldsymbol{u} + 2\Omega\times\boldsymbol{u} = -\frac{\nabla p}{\rho_f} + \nu\Delta\boldsymbol{u} + \boldsymbol{f}. \quad (1)$$

Here, ρ_f and ν are the density and the kinematic viscosity of the fluid, respectively, $2\Omega\times\boldsymbol{u}$ is the Coriolis force, and $\boldsymbol{f}$ is an external force. For an incompressible fluid, rotation breaks the statistical isotropy of the flow, but not its homogeneity. Note that the centrifugal force $\Omega\times\Omega\times(\boldsymbol{r}-\boldsymbol{r}_0)$, which depends on the distance from the position of the rotation axis $\boldsymbol{r_0}$, is absorbed in the pressure p, which is determined by the incompressibility condition $\nabla\cdot\boldsymbol{u}=0$. The regime of the flow is determined by the Reynolds number, Re_λ (see Table I), and by the Rossby number previously defined. When $\mathrm{Ro}\gg 1$, the turbulent motions have time scales much shorter than the rotation time scale τ_Ω, and the flow is almost unaffected by rotation. Rotation begins to affect the flow at $\mathrm{Ro}\sim O(1)$, when τ_Ω is of the order of the eddy turnover time at the forcing scale $1/(u_0 k_f)$. A characteristic scale of rotating turbulence is the Zeman wave number [9,43,44] defined as the Fourier scale where the inertial turnover time, $\tau_{\mathrm{nl}}(k)=\varepsilon^{-1/3}k^{-2/3}$, becomes of the same order of τ_Ω, i.e., $k_\Omega\sim(\Omega^3/\varepsilon)^{1/2}$, ε being the energy transfer rate. For $\mathrm{Ro}\le 1$, the dynamics of the energy transfer will be largely influenced by rotation. Importantly enough, as soon as the Zeman wave number is larger than k_f, an inverse energy transfer develops for $k\le k_f$, characterized by a strong accumulation of the kinetic energy into 2D large-scale structures. As a result, for $\mathrm{Ro}\le 1$, the system develops a forward cascade of energy, partially affected by the presence of rotation, and a simultaneous inverse energy cascade leading to a strong anisotropy. The need to resolve both interval of scales is the major bottleneck for direct numerical simulations.

In the reference frame rotating with angular frequency Ω, the equations for the trajectory $\boldsymbol{r}_t$ and the velocity $\boldsymbol{v}(\mathbf{r}_t,t)$ of a small sphere of radius R and density ρ_p suspended in the fluid field $\boldsymbol{u}$ can be approximated as [45]

$$\dot{\boldsymbol{r}}_t = \boldsymbol{v}, \quad (2)$$

$$\dot{\boldsymbol{v}} = \beta D_t\boldsymbol{u} - \frac{1}{\tau_p}(\boldsymbol{v}-\boldsymbol{u}) - 2\Omega\times(\boldsymbol{v}-\beta\boldsymbol{u}) - (1-\beta)\{\Omega\times[\Omega\times(\boldsymbol{r}_t-\boldsymbol{r}_0)]\}, \quad (3)$$

where $\boldsymbol{r}_0$ is the position of the rotation axis. Within the point-particle model, the inertial dynamics is controlled by two nondimensional parameters, the density ratio, $\beta=3\rho_f/(\rho_f+2\rho_p)$, and the Stokes number, $\mathrm{St}=\tau_p/\tau_\eta$, defined as the ratio between the particle relaxation time, $\tau_p=R^2/3\beta\nu$, and the Kolmogorov time τ_η. The first term on the rhs of Eq. (3) is the fluid acceleration and results from an estimate of the added-mass and pressure gradients along the trajectory of the tracers. The second term is the Stokes drag. With respect to the case of homogeneous

TABLE II. Lagrangian dynamics parameters. $\beta = 3\rho_f/(\rho_f + 2\rho_p)$, ratio of the fluid and the particle densities; $\mathrm{St} = \tau_p/\tau_\eta$, Stokes number. We evolve ten different families of inertial particles, plus a family of tracers. An ensemble of $N_a = 5 \times 10^5$ particles for each family is injected on 128 different rotation axis, located in different positions inside the simulation volume. Additionally, a set of $N_r = 4 \times 10^6$ particles per family is uniformly injected in the flow, in order to optimize the statistical sampling of the whole simulation volume.

Family	β	St	Type
$T0$	...	...	Tracer
$H1$	0.4	0.3	Heavy
$H2$	0.4	0.7	
$H3$	0.8	0.3	
$H4$	0.8	0.7	
$L5$	1.2	0.3	Light
$L6$	1.2	0.7	
$L7$	1.6	0.3	
$L8$	1.6	0.7	
$L9$	1.6	1	
$L10$	1.6	5	

and isotropic flows, two new forces appear in the rhs: the Coriolis and the centrifugal or centripetal, the third and fourth terms, respectively. To our knowledge, this is the first attempt to assess the effects of these two forces on the statistical and dynamical properties of inertial particles in turbulence. At variance with the NSE for the flow, the centrifugal force is present in the equation for the particle motion and it explicitly breaks homogeneity because of its dependency on the distance from the rotation axis. Its sign depends on the factor $(\beta - 1)$: for heavy particles $(0 \leq \beta < 1)$ the force is centrifugal, while for light particles $(1 < \beta \leq 3)$ it is centripetal.

In Eq. (3), we neglect the Basset history and gravity forces and the Faxen corrections; moreover, we approximate the material derivative along the inertial particle trajectories in terms of the material derivative along tracer paths. In the previous setup, tracer trajectories are evolved according to the equation $\dot{\boldsymbol{r}}_t = \boldsymbol{u}(\boldsymbol{r}_t, t)$.

B. Direct numerical simulations setup

We perform a set of state-of-the-art high-resolution direct numerical simulations of the NSE in a periodic, cubic domain of size $L = 2\pi$ with up to $N^3 = 4096^3$ collocation points. The rotation axis is in the x direction; i.e., $\boldsymbol{\Omega} = (\Omega, 0, 0)$. The integration of Eq. (1) has been performed by means of a fully dealiased pseudospectral code, with the second-order Adams-Bashforth scheme with viscous term exactly integrated. The parameters of the Eulerian dynamics for the different runs are reported in Table I. The integration of Eq. (2) is performed by interpolating the Eulerian velocity field and its derivatives with a sixth-order B-spline algorithm on the particle position [46]. The parameters of the Lagrangian dynamics can be found in Table II. At high rotation, the presence of a simultaneous forward and inverse cascade asks for an optimized setup, to minimize spurious finite-size effects. The *critical* Rossby number where energy starts to flow upscale is known or believed to depend on the way the system is forced [21,22,47] and on the aspect ratio of the volume where the flow is confined [16,28,48]. In the presence of an inverse flux, it is crucial to force the system at intermediate wave numbers to allow the large-scale flow to develop its own dynamics, without being directly influenced by the forcing. Moreover, an energy sink mechanism must be added to prevent the formation of a condensate at the lowest Fourier mode that could spoil the statistics at all scales.

To match the previous requirements, we adopt a stochastic isotropic Gaussian force $\boldsymbol{f}$, active on a narrow shell of wave numbers at $k_f \in [4{:}6]$. The vector of each forcing Fourier mode is obtained as $\mathbf{f}(\mathbf{k}, t) = f_0(i\mathbf{k} \times \mathbf{X}(t))$. The variables $X_i(t)$ are an independent, identically distributed time-differentiable stochastic processes, solution of the following Ornstein-Uhlenbeck second-order process:

$$dX_i(t) = -\left(\frac{1}{\tau_f} X_i(t) - \frac{1}{8\tau_f^2}\int_0^t X_i(t')dt'\right)dt + \sqrt{\frac{1}{4\tau_f^3}}dW_i(t). \tag{4}$$

In the expression above, τ_f is the correlation time of the process and $W_i(t)$ is a Wiener process. It is important to stress that the above time-correlated process ensures the continuity of the Lagrangian acceleration of the tracers (see Ref. [49] for details). At low Rossby number, to arrest the inverse cascade, we remove energy at large scales with a linear friction term $\alpha\Delta^{-1}\boldsymbol{u}$ and acting on wave numbers $|\boldsymbol{k}| \leq 2$ only. This term is added to evolve the Lagrangian particles on a stationary state without the need to overresolve the field in the infrared regime.

To understand the basic phenomenology of a rotating turbulent flow, it is useful to recall the different dynamical states that can be observed in the case of strong rotation, i.e., low Rossby number. In Fig. 3, we show the temporal evolution of the total kinetic energy, $E_{\mathrm{kin}} = \int d\boldsymbol{p}|\boldsymbol{u}_{\boldsymbol{p}}|^2$, starting from a fluid at rest and until a stationary regime is achieved. In the early stage, the rotation rate Ω is zero, and the flow develops a 3D direct cascade. Small-scale thermalization is indicated by the overshoot of the kinetic energy. This is the standard situation of stationary, nonrotating turbulent flows where the energy input is balanced by viscous dissipation. After this stage, we switch on the rotation and the inverse energy cascade starts to develop if Ω is large enough: this is indicated by the linear growth in time of the kinetic energy. Later, we switch on the damping

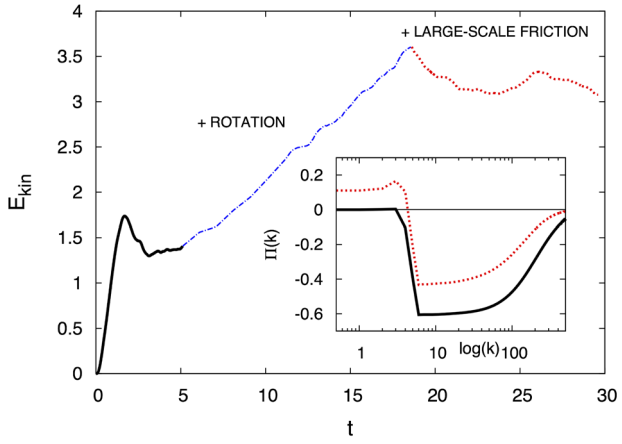

FIG. 3. Kinetic energy evolution for a typical run with large rotation rate, in the presence of an inverse energy cascade. We show the thermalization regime when rotation is not applied (black continuous line), the inverse cascade regime after rotation is switched on (blue dashed line), and the stationary regime obtained by the application of a large-scale friction (red dotted line). Inset: Kinetic energy flux measured at the two stationary regimes: without rotation (black continuous line) and with rotation and large-scale friction (red dashed line), in the DNS with large rotation rate $\Omega = 10$.

term at large scale. Doing that, we end up with a statistically stationary regime for a strongly rotating turbulent flow.

In the inset of Fig. 3, we show the presence of a simultaneous positive and negative spectral flux when the rotation rate is large enough, indicating the existence of a forward and inverse energy transfer at scales smaller and larger of the forcing scale, respectively. We remark that the spectral flux is here defined as the transfer of energy across a wave number k by the nonlinear interactions $\boldsymbol{N}_{\mathbf{p}}$ of the Navier-Stokes equations [50]: $\Pi(k) = \int_{|p|<k} d\boldsymbol{p}\boldsymbol{u}^*_{\mathbf{p}} \cdot \boldsymbol{N}_{\mathbf{p}}$. The simultaneous presence of direct and inverse cascades is shown by the two plateaus in the spectral flux, in agreement with previous findings [16,20,48,51–54].

Once the turbulent flow is stationary, we seed it with Lagrangian particles of different inertia, released with the same velocity of the underlying fluid. When Ro is small, the flow is characterized by the presence of few intense columnar cyclones, corotating with Ω. In the plane perpendicular to the rotation, the associated two-dimensional vortices are much slower than any other structure in the flow. Moreover, as shown in Fig. 2, these cyclones strongly influence the distribution of the particles. Light particles are trapped inside, while heavy particles are ejected, leading to an extreme, singular preferential sampling of the underlying flow (see Sec. IV). In all cases we investigate here, the flow displays a few big cyclones well separated from each other. The breaking of the cyclone-anticyclone symmetry is a well-known feature of rotating turbulence [22,55–59]. It is also the indication that the formation of the vortical columnar structures cannot be entirely due to a 2D inverse cascade regime, because in the plane perpendicular to the rotation axis the symmetry is not broken. Nevertheless, it is suggestive to interpret the presence of three long-living coherent columns in terms of the dynamics of point vortices, since a system of three equal-sign point vortices is linearly stable in two dimensions [60]. We cannot exclude that the columnar vortices would eventually merge into a single cyclone, after long enough time. Considering that vortices with equal sign repel each other, and that their merging would cause the generation of an intense shear between them, it is arguable that the process of a collapse is unlikely to occur.

III. EULERIAN STATISTICS

A. Fourier analysis

Rotation affects the spectral distribution of the kinetic energy on a wide range of scales. For Fourier modes

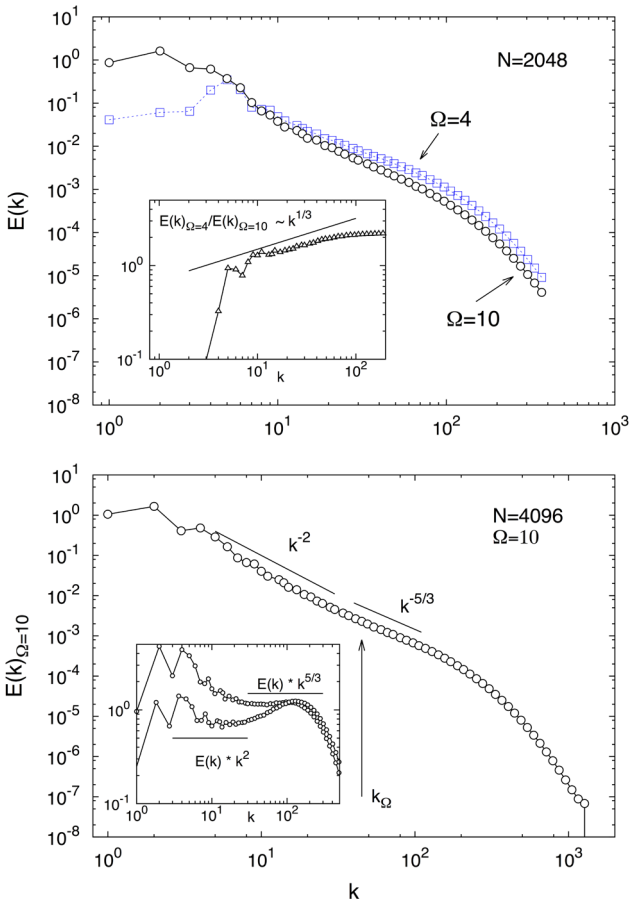

FIG. 4. Log-log plots of the energy spectrum. Top: Spectra for the runs at $N = 2048$. Data with $\mathrm{Ro} = 0.76$ and $\Omega = 4$ (squares) and data with $\mathrm{Ro} = 0.25$ and $\Omega = 10$ (circles). Inset: Effect of rotation on the forward energy cascade is highlighted in terms of the ratio of the two spectra, $E_{\Omega=4}(k)/E_{\Omega=10}(k) \sim k^{1/3}$. Bottom: Spectrum for $N = 4096$, $\mathrm{Ro} = 0.25$, and $\Omega = 10$; the expected scaling behaviors $\propto k^{-2}$ and $\propto k^{-5/3}$, above and below the Zeman wave number k_Ω, respectively, are also plotted. Inset: Spectrum for $N = 4096$ and $\Omega = 10$ compensated with k^{-2} and with $k^{-5/3}$.

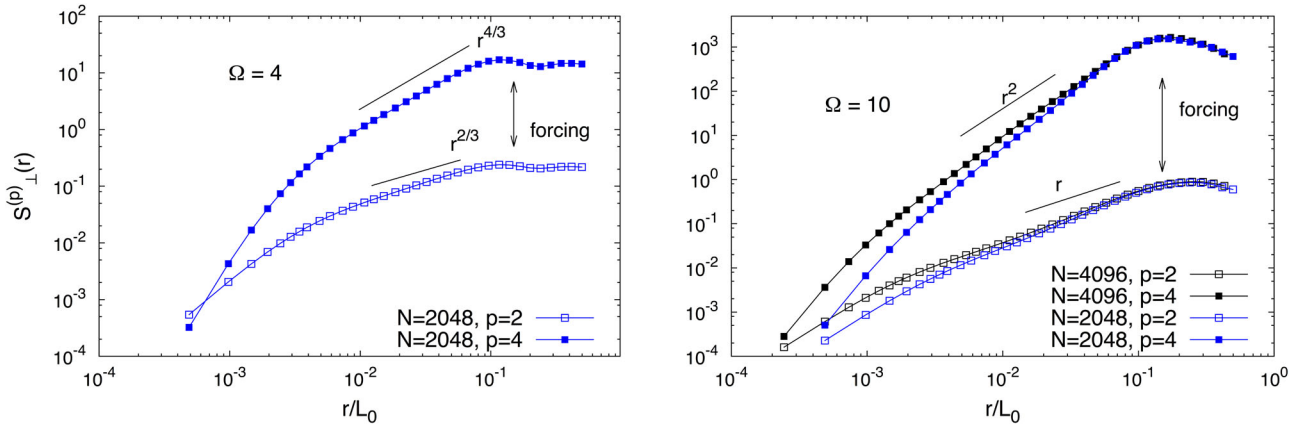

FIG. 5. Log-log plot of the second- $S_\perp^{(2)}(r)$ and fourth-order $S_\perp^{(4)}(r)$ Eulerian transverse structure functions. Left: Case with $N = 2048$ and $\Omega = 4$. The dimensional scaling predictions $\propto r^{p/3}$ according to the K41 isotropic scaling are also plotted. Right: Case with $N = 4096$, 2048 and $\Omega = 10$. The dimensional scaling prediction $\propto r^{p/2}$ is also plotted.

between the forcing and the Zeman wave numbers, $k_f < k < k_\Omega$, a standard phenomenological argument predicts for the energy spectrum:

$$E(k) = \int_{|\boldsymbol{p}|=k} d\boldsymbol{p} \langle |\boldsymbol{u}_{\boldsymbol{p}}|^2 \rangle \sim (\Omega\varepsilon)^{1/2} k^{-2}, \tag{5}$$

which is obtained by estimating the typical transfer time in terms of the nonlinear time and the rotation time $\tau_{\rm tr}(k) \propto \tau_{\rm nl}(k)^2/\tau_\Omega(k)$ [61–63]; see Ref. [27] for possible phenomenological extensions that also take into account anisotropic contributions. For small Rossby, $\Omega = 10$, and at small wave numbers, $k < k_f$, we observe the development of an inverse energy transfer: evidence is given in the top panel of Fig. 4, where we compare two spectra at low and high Rossby numbers, for the cases of resolution $N^3 = 2048^3$. At larger wave numbers, $k > k_f$, rotation causes a steepening of the energy spectrum in good qualitative agreement with the prediction Eq. (5). Note that when rotation is strong, $\Omega = 10$, the computed Zeman wave number is $k_\Omega \simeq 48$, indicating that presumably rotation has weaker effects at very large wave numbers towards the dissipative range.

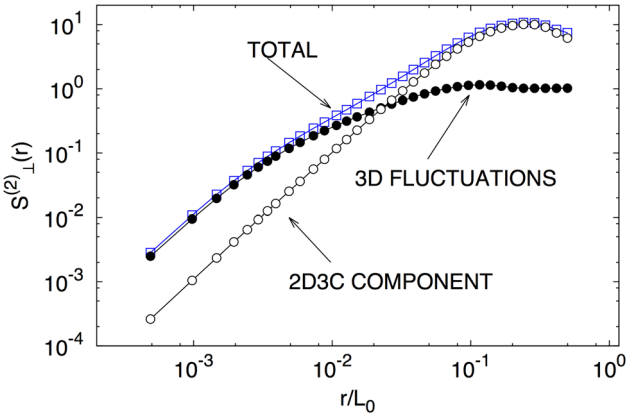

FIG. 6. Log-log plot of the second-order Eulerian transverse structure function in the plane perpendicular to the rotation axis, $S_\perp^{(2)}(r)$, for $N = 2048$ and $\Omega = 10$. Whole field $\boldsymbol{u}(x, y, z)$ (squares), to the 2D3C $\boldsymbol{u}_{\rm 2D}(y, z)$ component (empty circles), and to the fluctuating 3D component $\boldsymbol{u}'(x, y, z)$ (filled circles).

On the other hand, for large values of the Rossby number, $\Omega = 4$ and $k_\Omega \simeq 7$, the classical Kolmogorov scaling $E(k) \sim \varepsilon^{2/3} k^{-5/3}$ associated with the direct cascade is observed, and no backward energy transfer for $k < k_f$ develops. Remarkably enough, the change in the spectral exponent that takes place by varying the Rossby number can be better identified by plotting the ratio of two spectra, $E_{\Omega=4}(k)/E_{\Omega=10}(k) \propto k^{-5/3}/k^{-2}$: when this is done, a clear $\simeq k^{1/3}$ behavior is observed (see the inset of Fig. 4). In the bottom panel of the figure, we show the energy spectrum at $N^3 = 4096^3$ resolution for the small Rossby number regime, $\Omega = 10$. The resolution is now sufficient to detect the transition from the k^{-2} to $k^{-5/3}$ scaling around the Zeman wave number, as can be better appreciated in terms of the compensated plots in the inset of Fig. 4. These results are in agreement with previous numerical findings [64,65].

The analysis in terms of the spectral properties cannot be considered conclusive. Spectra are not sensitive to the Fourier phases, and, therefore, they are unable to distinguish if the two-point spatial correlation is the result of a stochastic turbulent background or the result of coherent structures. Moreover, in the presence of different physical scaling ranges (inverse cascade for $k < k_f$, direct cascade plus rotation for $k_f < k < k_\Omega$, and direct cascade with Kolmogorov phenomenology for $k > k_\Omega$), it is impossible to detect power laws as a function of the wave number, even at the highest resolution ever achieved, as shown here. Finally, and more importantly, in order to assess the relative importance of coherent and background fluctuations, it is mandatory to move to the real-space analysis, such as to

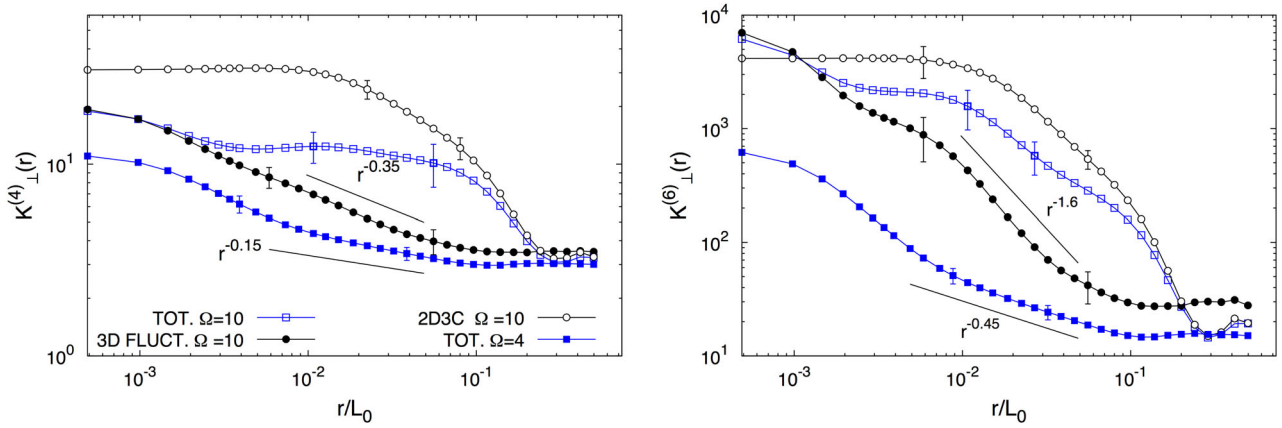

FIG. 7. Left: Log-log plot of the fourth-order flatness $K^{(4)}_\perp(r)$ derived from the Eulerian structure functions transverse to the rotation axis, for data with $N = 2048$. Data from DNS with large rotation rate, in the presence of an inverse cascade ($\Omega = 10$, Ro $= 0.25$): full field $\boldsymbol{u}$ (empty squares); 2D3C $\boldsymbol{u}_{2D}$ component (empty circles); fluctuating 3D component $\boldsymbol{u}'$ (filled circles). Data from DNS with the direct cascade only, and no-columnar vortices ($\Omega = 4$, Ro $= 0.76$): full field $\boldsymbol{u}(x, y, z)$ (filled squares). We also superpose the power - law prediction $\propto r^{-0.15}$ obtained from independent measurements of isotropic turbulence without rotation and the best fit for the power law measured with intense rotation in the present data $\propto r^{-0.35}$. Right: The same for the sixth-order flatness $K^{(6)}_\perp(r)$ (same symbols). Error bars are estimated from different velocity snapshots and shown for a representative subset of points.

have a direct way to assess intermittency and deviations from Gaussian statistics scale by scale and for high-order velocity correlations.

B. Real-space analysis

A fundamental issue of rotating turbulence is to find suitable observables that can disentangle the coupling between the 2D3C slow modes and the 3D fast modes. A natural expectation is that the strongest effects of the columnar vortices might manifest in the statistics of the increments of the velocity components perpendicular to Ω: $\delta u(r)_\perp = [(\boldsymbol{u}(\boldsymbol{x}+\boldsymbol{r}) - \boldsymbol{u}(\boldsymbol{x})] \cdot \hat{\boldsymbol{t}}$, where the distance $\boldsymbol{r}$ is in the plane normal to Ω, and the versor $\hat{\boldsymbol{t}}$ is orthogonal to both Ω and $\boldsymbol{r}$. Thus, we define the pth order transverse structure function as

$$S^{(p)}_\perp(r) = \langle (\delta u(r)_\perp)^p \rangle, \tag{6}$$

where isotropy is assumed in the normal plane. In Fig. 5, we show the second- and the fourth-order transverse structure function for runs at different Reynolds and Rossby numbers. The scaling behaviors indicate the existence of two different regimes in the inertial range of scales, $\eta < r < \ell_f$. In the right-hand panel, we show data at small Ro ($\Omega = 10$), and for two different Reynolds numbers. A qualitative agreement with the dimensional scaling $\propto r^{p/2}$ corresponding to the Zeman phenomenology [29,66] is observed at large scale, while small scales depend on the Reynolds number and display a change in the local slope by approaching the viscous scale at the highest resolution. At high Rossby number ($\Omega = 4$, left-hand panel of Fig. 5), rotation effects are always subleading. Here, the statistics is in good agreement with the Kolmogorov K41 prediction [50]. At Ro $\ll 1$, the scaling laws are always spoiled by anisotropy and the only systematic way to disentangle scaling properties would be to resort to a decomposition in terms of eigenfunctions of the group of rotations [67,68]. Moreover, the flow is naturally bimodal, with a 2D3C dynamics superposed and entangled with the 3D turbulent fluctuations.

To better clarify the statistics scale by scale, we propose to decompose the velocity field into two components, one given by the 2D3C slow modes and the other associated to the 3D fast modes:

$$\boldsymbol{u}(x, y, z|t) = \boldsymbol{u}_{2D}(y, z|t) + \boldsymbol{u}'(x, y, z|t). \tag{7}$$

Here, we define the two-dimensional field as the average of the velocity field in the direction of Ω: $\boldsymbol{u}_{2D}(y, z|t) = \int dx \boldsymbol{u}(x, y, z|t)$. In Fig. 6, we plot the second-order transverse structure function $S^{(2)}_\perp(r)$ measured for the undecomposed field and for the two fields obtained by the above decomposition. The figure shows the existence of a scale, of the order of $l_\Omega = 2\pi/k_\Omega$, where the statistics changes from being 2D3C to 3D dominated. The background field follows quite closely the Kolmogorov scaling $\propto r^{2/3}$ (not shown), while the 2D3C field has a scaling much smoother than the Zeman estimate. This does not necessarily contradict the results of Sec. III A. Rather, it clearly shows that within the Eulerian statistics, there are two different components that influence the physics at different scales. It also suggests that any attempt to fit or predict scaling laws without a separation of the different contributions might lead to uncontrolled approximations.

In Fig. 7, we plot the fourth-order (left-hand panel) and sixth-order (right-hand panel) flatness derived from the transverse structure functions,

TABLE III. Best fit to the scaling exponents of the pth-order flatness, $K_\perp^{(p)}(r) \propto r^{\zeta(p)}$, with $p = 4$, 6. For the high rotation $\Omega = 10$, we fit the scaling for the fluctuating part only (filled circles in Fig. 7). For the case at low rotation rate $\Omega = 4$, we fit the data for the whole undecomposed field because it coincides with the fluctuations (no vortical structures). Error refers to the uncertainty in the fit by changing the fitting scaling range.

	$\Omega = 4$	$\Omega = 10$
$\zeta(4)$	−0.15(2)	−0.35(5)
$\zeta(6)$	−0.45(5)	−1.6(1)

$$K_\perp^{(4)}(r) \equiv \frac{S_\perp^{(4)}(r)}{[S_\perp^{(2)}(r)]^2}, \qquad K_\perp^{(6)}(r) \equiv \frac{S_\perp^{(6)}(r)}{[S_\perp^{(2)}(r)]^3},$$

for the undecomposed velocity field, the 2D projection, and the fluctuating part. Except for very large spatial increments, the curves are always far from the Gaussian limit. Consider the data for the whole field at large rotation rate, i.e., $\Omega = 10$ (empty squares in both panels). The fourth-order flatness displays a weak dependence on the analyzed scale in the inertial range, while the sixth-order flatness does change for scales smaller than the forcing range. How much are the observed deviations from a Gaussian behavior due to the presence of the vortical columnar structures, and how much are they due to the 3D turbulent fluctuations?

If we consider separately the statistics of the 2D3C component $\boldsymbol{u}_{2D}$ (empty circles) and the statistics of the 3D fluctuations $\boldsymbol{u}'$ (filled circles) (in Fig. 7), we find a surprising result. The fourth-order flatness of the fast modes exhibits a strong scale dependence. A scale-dependent flatness is the signature of intermittency: here, we observe it for both the 3D rapidly fluctuating velocity field and, to a smaller extent, the 2D3C slowly varying component. The same trend is observed for the sixth-order flatness. These results reveal that the reduction of intermittency previously reported from data at smaller resolution and without a scale-by-scale analysis [33,65,69,70] is merely apparent and probably due to a nontrivial combination of effects induced by the coherent structures and contributions from the underlying 3D turbulent fluctuations. This is one of the main results of this paper.

Finally, we note that naively one would expect that the flatness of the fluctuating field for $\Omega = 10$ should be equal to the flatness of the total field for $\Omega = 4$ (filled squares). Our data show that this is not the case, meaning that rotation not only leads to the formation of the 2D columnar structures, but also modifies the 3D fluctuating turbulence, if the Rossby number is small enough. We summarize in Table III the results for the best fit to the flatness scaling exponents for the fluctuating components at high rotation and for the total component at small rotation rates.

IV. LAGRANGIAN STATISTICS

A novel way to investigate the statistics of the columnar vortices is to exploit the peculiar features of the inertial particles in sampling the flow. It is known that light particles are attracted inside the vortices, while heavy particles are expelled out of them [39,71]. By studying the velocity statistics measured along the trajectories of particles with different inertia, it is possible to use their preferential concentration in specific flow regions, to enhance or deplete the contribution of the slow vortical modes with respect to the turbulent background.

Here, we start by analyzing the different contributions of the forces that influence inertial particles' motion. In Fig. 8, we plot the time evolution of the root-mean-squared values of all accelerations:

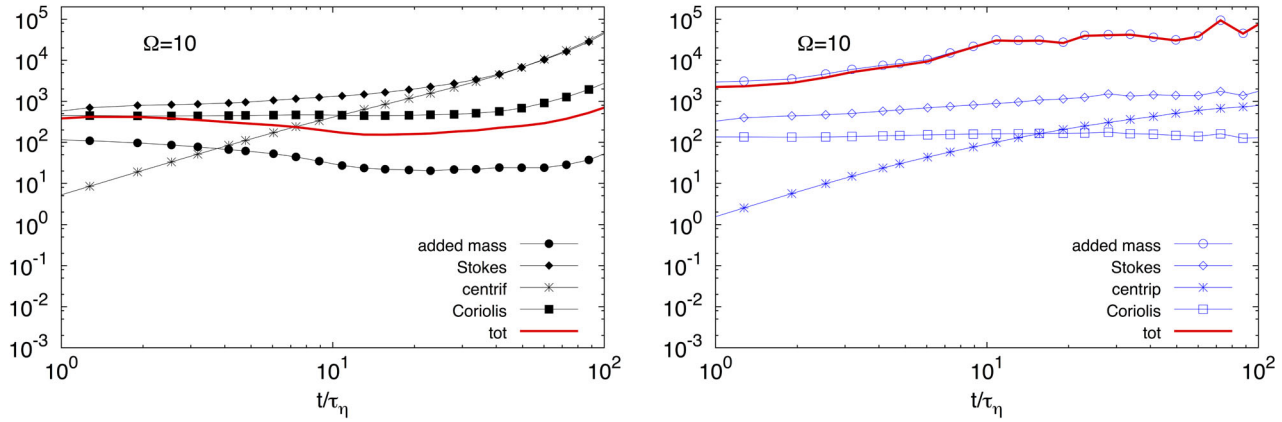

FIG. 8. Log-log plot of the time evolution of the contribution of the different forces to the rms particle acceleration, at resolution $N = 2048$ and for high rotation (low Rossby number). Left: Inertial heavy particles, with $\beta = 0.4$ and $\mathrm{St} = 0.7$ (family $H2$ in Table II). Right: Inertial light particles, with $\beta = 1.6$ and $\mathrm{St} = 0.7$ (family $L8$ in Table II).

$$\begin{cases} a^{\rm tot}_{\rm rms}(t) = \langle \dot{\boldsymbol{v}}^2 \rangle, & \text{total,} \\ a^{\rm am}_{\rm rms}(t) = \beta^2 \langle (D_t \mathbf{u})^2 \rangle, & \text{added mass,} \\ a^{\rm St}_{\rm rms}(t) = 1/\tau_p^2 \langle (\mathbf{v}-\mathbf{u})^2 \rangle, & \text{Stokes drag,} \\ a^{\rm Co}_{\rm rms}(t) = 4 \langle [\Omega \times (\mathbf{v}-\beta \mathbf{u})]^2 \rangle, & \text{Coriolis,} \\ a^{\rm Cp}_{\rm rms}(t) = (1-\beta)^2 \langle [\Omega \times (\Omega \times (\mathbf{r}_t - \mathbf{r}_0)]^2 \rangle, & \text{centripetal.} \end{cases} \tag{8}$$

When the Rossby number is small, i.e., for $\Omega = 10$, the inertial particle dynamics does not always attain a statistically steady state. The relative importance of the forces is affected for two different reasons. The first one is purely kinematic, since both Coriolis and centripetal forces are proportional to the rotation rate. The second one is dynamical: the organization of the flow, with the formation of strong columnar vortices, competes with the kinematic effects.

If particles are heavier than the fluid, the centrifugal force soon becomes dominant: particles not only tend to avoid coherent vortical structures, but also tend to spiral away from their rotation axis very efficiently (see also Fig. 2). This enhanced centrifugal action is balanced by the Stokes drag only. Comparing, $a^{\rm St}_{\rm rms}$ and $a^{\rm Cp}_{\rm rms}$, it is interesting to note that this balance is very efficient, leading to a total acceleration $a^{\rm tot}_{\rm rms}$ much smaller than the single contributions, and to an almost stationary statistics in the long-time limit. In this regime, the dynamics of the heavy particles is uncorrelated with respect of the underlying fluid. Particles move away from their rotation axis with a spiral motion, whose radius grows exponentially in time, $r(t) \sim \exp(\Omega^2 \tau_p t)$. Since their velocity also increases exponentially over time, the particle Reynolds number might eventually become too large for the validity of the model equations [Eqs. (2) and (3)] [45]. Hence, it would be crucial to perform a systematic comparison with experimental data, in order to understand the limitation of the pointlike approach in the limit of very heavy particles.

For small Rossby number, we observe an opposite behavior in the case of light particles. The centripetal force attracts the light particles toward their original rotation axis, but its intensity vanishes as $r_t \to r_0$. The overall effect is, therefore, to spatially confine the trajectories of light particles, depleting turbulent diffusion and preventing them from exploring regions far away from the rotation axis. Additionally, one needs to consider the dynamical attraction inside the coherent vortical structures. As visually shown in Fig. 2, preferential centripetal concentration is the leading effect and almost all light particles are trapped inside vortical structures. The leading term in light particles acceleration is the added mass, which is not balanced by other forces. We also notice that at long times the temporal behavior of the added-mass term becomes noisy, in spite of the large number of particles used in computing the average. This is because eventually all light particles collapse into the cores of a few columnar vortices, thus reducing the effective statistics.

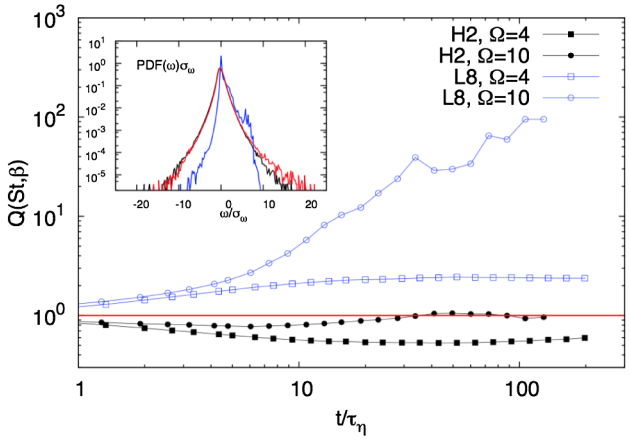

FIG. 9. A measure of the inertial particles' preferential sampling of the vorticity regions at low, $\Omega = 4$, and high, $\Omega = 10$, rotation rates for two different families: a heavy one $H2$ and a light one $L8$. Inset: For the case with $\Omega = 10$, the probability density function of the vertical vorticity ω_x normalized to its standard deviation, as measured at the positions of light particles $L8$ (blue), heavy particle $H2$ (black), and tracers $T0$ (red). Data refer to DNS at resolution $N = 2048$.

The singular role played by the presence of the coherent structures for Lagrangian statistics is better quantified in Fig. 9, where we plot the preferential sampling of specific flow regions, by measuring the average vertical vorticity at the particle positions normalized with the averaged vertical vorticity in the volume:

$$Q_{{\rm St},\beta}(|t) = \frac{\langle [w_x(\mathbf{r}_t, t)]^2 \rangle_{\beta,{\rm St}}}{\langle [w_x(\mathbf{r}_t, t)]^2 \rangle_{\rm tracer}}. \tag{9}$$

At low rotation, $\Omega = 4$, the preferential sampling by heavy or light particles is similar to that observed in homogeneous and isotropic turbulence, and quantitatively it is an $O(1)$ effect with respect to the mean-fluid vorticity. At large rotation rate, the situation is different: heavy particles, because of the sweeping due to the centrifugal forces, do not show preferential concentration, while light particles oversample the intense vorticity regions with an effect that is a factor $O(100)$ larger. In Fig. 9, we also show the probability distribution function (PDF) of the vertical vorticity w_x along particle trajectories for tracers and for one light and one heavy family. Notice the bimodal PDF for the light particles induced by the trapping in the vortex cores; for the heavy particles, the PDF is symmetric, because of the homogeneous sampling of the flow regions outside strong vortical structures.

Concerning absolute dispersion, the influence of the strong vortical structures will induce a systematic anisotropic effect for tracers [41]. On the other hand, since the vortical structures are fatal traps for the light particles and

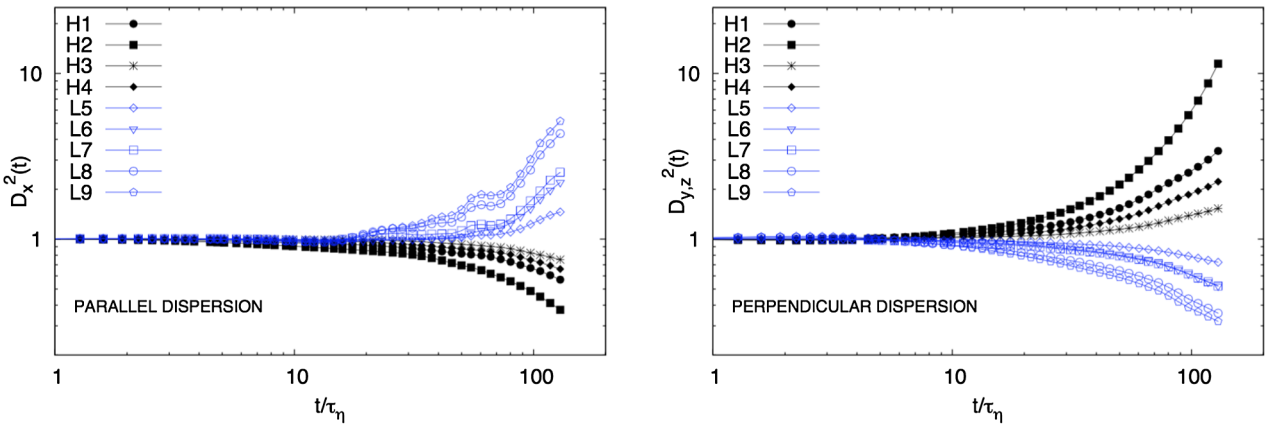

FIG. 10. Absolute dispersion of inertial particles in the direction parallel (left) and perpendicular (right) to the rotation axis. The mean-square displacement of inertial particles is normalized with that of tracers. Labels refer to the four families of heavy particles $H1$–$H4$ and to the five families of light particles $L5$–$L9$. See Table II for details. Data refer to the DNS with $N = 2048$ and $\Omega = 10$.

strong repellers for heavy particles, we expect to measure strong deviations in the single-particle dispersion, too. In Fig. 10, we show the mean-square absolute dispersion of the particles from their initial position as a function of time,

$$D^i_{\mathrm{St},\beta}(t) = \frac{\langle (r^i_t - r^i_0)^2 \rangle_{\mathrm{St},\beta}}{\langle (r^i_t - r^i_0)^2 \rangle_{\mathrm{tracer}}}, \tag{10}$$

along different directions $i = (x, y, z)$, here normalized with the ones measured for tracers. For the heavy particles, we find that the diffusion in the plane normal to the rotation axis Ω is enhanced, due to the centrifugal effect, while parallel diffusion is reduced. Moreover, at a fixed value of the density mismatch β, the effect is stronger for higher Stokes number.

The diffusion behaviors are inverted for light particles. The trapping in the vortices strongly suppresses the transverse diffusing, but enhances the one parallel to the rotation axis (see also Fig. 2). Because of the two dimensionalization induced by rotation, all the components of the fluid velocity are weakly dependent on the coordinate along the rotation axis. This occurs also for the component of the velocity parallel to Ω. As a result, the columnar vortices can have a uniform coherent velocity in the direction of Ω. Light particles, once trapped in the columnar structures, are transported almost ballistically along their axis, as in an elevator.

V. CONCLUSIONS

Rotating turbulence is key for many industrial and geophysical applications. In many empirical setups, it is also key to control the dispersion and advection of particles. Very little is known concerning the combined Eulerian-Lagrangian properties, and a long-lasting debate exists concerning the effects of confinement and forcing, and whether or not they have a singular footprint on the statistics. We present the results of a state-of-the-art direct numerical simulation study of Eulerian and Lagrangian rotating turbulence at high and low Rossby numbers. To our knowledge, this is the first attempt to study the evolution of particles in rotating turbulence and in the presence of both direct and inverse energy cascade. At high rotation rates, we show that the Eulerian ensemble strongly deviates from a self-similar normal-distributed statistics at changing the analyzed scale, with a key influence of the coherent vortical columnar structures. By removing from the velocity field the 2D3C component, obtained by averaging over the vertical direction, we are able to assess quantitatively the degree of intermittency present in the remaining 3D fluctuations: in particular, we show that there exists a nontrivial non-Gaussian contribution also in the background fluctuations. Whether this result is specific to an intermediate range of Rossby numbers and Eulerian intermittency might or not decrease in the limit of very small Rossby number is a question that needs further investigation. We simultaneously measure the Lagrangian statistics, following millions of light or heavy and tracer particles injected in different rotation axes inside the rotating volume. We show, for the first time, that an extreme preferential sampling develops as soon as there exists coherent structures in the flow and that this has a singular effect for the fate of heavy or light particles. In particular, heavy particles diffuse more efficiently in the plane perpendicular to the rotation axis, while light particles tend to diffuse only vertically. The discovery of this elevator effect might have important implications for industrial applications and for the population dynamics of passive or active microswimmers in the oceans. Tracking light particles is also key to highlighting the breaking of cyclonic-anticyclonic symmetry, a property of any 3D rotating fluid at Rossby numbers $O(1)$. Many issues remain open. It would be extremely interesting to understand the degree of universality of the 2D3C statistics and of the

remaining 3D fluctuations at changing the forcing mechanisms, the large-scale friction (and the confinement aspect ratio). It is also expected, but not measured yet, that the vortical structures will strongly influence the two-particles Richardson dispersion in rotating flow. Similarly, it is not known how much Lagrangian velocity increments along particles' trajectories are eventually affected by rotation, a key point to build up stochastic models for particles' dispersion in atmospheric and marine environments. A detailed study of single-particle and two-particles (relative dispersion) diffusion statistics is a next step in Lagrangian dynamics exploration.

It is still an open question to understand how to match the results from finite volume experiments and direct numerical simulations with the predictions of unforced wave turbulence in infinite domains (see also Ref. [72] for a discussion of discreteness and resolution effects). Finite volume effects can be estimated by comparing the typical distance traveled by the waves during the duration of the simulation, estimated in terms of their group velocity. In our case, for the highest rotation case this distance is pretty small, of the order of 10% of the total volume. Using state-of-the-art highly resolved DNS, as done here, is crucial in order to reduce the spectral gap with the horizontal plane also. Here, for the highest resolved case, we have an excellent resolution of the buffer layer near $k_{||} = 0$, including wave numbers with angle close to 0.04 deg with the horizontal plane and thus reducing finite volume effects. However, improving angular resolution to better capture the spectral buffer layer also at small wave numbers close to the two-dimensional manifold is an issue [26]: further numerical investigations, e.g., in slab geometries, permitting one to obtain values of $k_{||} = 0$ small enough are desirable to shed further light on the problem of 2D-3D modes coupling.

Other numerical approaches meant to understand the importance of different triadic interactions in Fourier space, and to further clarify the nature of the inverse cascade in purely rotating turbulence, are possible. One important example is given by Ref. [73], where reduced Navier-Stokes equations including only near-resonant, nonresonant, and near-two-dimensional triad interactions are considered. These numerical approaches are restricted to work on spectral space, with severe limitation in the number of modes that can be considered.

ACKNOWLEDGMENTS

Simulation has been performed at CINECA, within the PRACE Grant No. Pra092256. We acknowledge the European COST Action MP1305 "Flowing Matter" and funding from the European Research Council under the European Union's Seventh Framework Programme, AdG ERC Grant Agreement No. 339032. A. S. L. acknowledges support from MIUR, within projects PESCA SSD and RITMARE. This work is part of the research program of the Foundation for Fundamental Research on Matter (FOM), which is part of the Netherlands Organisation for Scientific Research (NWO).

[1] H. P. Greenspan, *The Theory of Rotating Fluids* (Cambridge University Press, Cambridge, England 1968).
[2] P. A. Davidson, *Turbulence in Rotating, Stratified and Electrically Conducting Fluids* (Cambridge University Press, CAmbridge, 2013).
[3] A. S. Barness, *An Assessment of the Rotation Rates of the Host Stars of Extrasolar Planets*, Astrophys. J. **561**, 1095 (2001).
[4] J. Y.-K. Cho, K. Menou, B. Hansen, and S. Seager, *Atmospheric Circulation of Close-In Extrasolar Giant Planets. I. Global, Barotropic, Adiabatic Simulations*, Astrophys. J. **675**, 817 (2008).
[5] H. Dumitrescu and C. Vladimir, *Rotational Effects on the Boundary-Layer Flow in Wind Turbines*, AIAA J. **42**, 408 (2004).
[6] H. J. Lugt, *Vortex Flow in Nature and Technology* (Wiley-Interscience, New York, 1983).
[7] L. S. Hodgson and A. Brandenburg, *Turbulence Effects in Planetesimal Formation*, Astron. Astrophys. **330**, 1169 (1998).
[8] A. Ogawa, *Mechanical Separation Process and Flow Patterns of Cyclone Dust Collectors*, Appl. Mech. Rev. **50**, 97 (1997).
[9] E. J. Hopfinger, F. K. Browand, and Y. Gagne, *Turbulence and Waves in a Rotating Tank*, J. Fluid Mech. **125**, 505 (1982).
[10] P. J. Staplehurst, P. A. Davidson, and S. B. Dalziel, *Structure Formation in Homogeneous, Freely Decaying, Rotating Turbulence*, J. Fluid Mech. **598**, 81 (2008).
[11] F. Moisy, C. Morize, M. Rabaud, and J. Sommeria, *Decay Laws, Anisotropy and Cyclone-Anticyclone Anisotropy in Decaying Rotating Turbulence*, J. Fluid Mech. **666**, 5 (2011).
[12] S. B. Dalziel, *The Twists and Turns of Rotating Turbulence*, J. Fluid Mech. **666**, 1 (2011).
[13] E. Yarom, Y. Vardi, and E. Sharon, *Experimental Quantification of Inverse Energy Cascade in Deep Rotating Turbulence*, Phys. Fluids **25**, 085105 (2013).
[14] B. Gallet, A. Campagne, P.-P. Cortet, and F. Moisy, *Scale-Dependent Cyclone-Anticyclone Asymmetry in a Forced Rotating Turbulence Experiment*, Phys. Fluids **26**, 035108 (2014).
[15] P. K. Yeung and Y. Zhou, *Numerical Study of Rotating Turbulence with External Forcing*, Phys. Fluids **10**, 289 (1998).
[16] L. Smith and F. Waleffe, *Transfer of Energy to Two-Dimensional Large Scales in Forced, Rotating Three-Dimensional Turbulence*, Phys. Fluids **11**, 1608 (1999).
[17] M. Thiele and W.-C. Müller, *Structure and Decay of Rotating Homogeneous Turbulence*, J. Fluid Mech. **637**, 425 (2009).
[18] K. Yoshimatsu, M. Midorikawa, and Y. Kaneda, *Columnar Eddy Formation in Freely Decaying Homogeneous Rotating Turbulence*, J. Fluid Mech. **677**, 154 (2011).

[19] T. Teitelbaum and P. D. Mininni, *The Decay of Turbulence in Rotating Flows*, Phys. Fluids **23**, 065105 (2011).

[20] Q. N. Chen, S. Y. Chen, G. L. Eyink, and D. D. Holm, *Resonant Interactions in Rotating Homogeneous Three-Dimensional Turbulence*, J. Fluid Mech. **542**, 139 (2005).

[21] A. Sen, P. D. Mininni, D. Rosenberg, and A. Pouquet, *Anisotropy and Nonuniversality in Scaling Laws of the Large-Scale Energy Spectrum in Rotating Turbulence*, Phys. Rev. E **86**, 036319 (2012).

[22] A. Alexakis, *Rotating Taylor-Green Flow*, J. Fluid Mech. **769**, 46 (2015).

[23] F. S. Godeferd and F. Moisy, *Structure and Dynamics of Rotating Turbulence: A Review of Recent Experimental and Numerical Results*, Appl. Mech. Rev. **67**, 030802 (2015).

[24] R. P. J. Kunnen, H. J. H. Clercx, and B. J. Geurts, *Vortex Statistics in Turbulent Rotating Convection*, Phys. Rev. E **82**, 036306 (2010).

[25] C. Cambon, N. N. Mansour, and F. S. Godeferd, *Energy Transfer in Rotating Turbulence*, J. Fluid Mech. **337**, 303 (1997).

[26] C. Cambon, R. Rubinstein, and F. S. Godeferd, *Advances in Wave Turbulence: Rapidly Rotating Flows*, New J. Phys. **6**, 73 (2004).

[27] F. Bellet, F. S. Godeferd, J. F. Scott, and C. Cambon, *Wave Turbulence in Rapidly Rotating Flows*, J. Fluid Mech. **562**, 83 (2006).

[28] J. F. Scott, *Wave Turbulence in a Rotating Channel*, J. Fluid Mech. **741**, 316 (2014).

[29] S. Galtier, *Weak Inertial-Wave Turbulence Theory*, Phys. Rev. E **68**, 015301 (2003).

[30] V. E. Zakharov, V. S. Lvov, and G. Falkovich, *Kolmogorov Spectra of Turbulence I: Wave Turbulence* (Springer, New York, 1992).

[31] S. Nazarenko, *Wave Turbulence* (Springer, Berlin, 2011).

[32] A. C. Newell and B. Rumpf, *Wave Turbulence*, Annu. Rev. Fluid Mech. **43**, 59 (2011).

[33] C. N. Baroud, B. B. Plapp, H. L. Swinney, and Z. S. She, *Scaling in Three-Dimensional and Quasi-Two-Dimensional Rotating Turbulent Flows*, Phys. Fluids **15**, 2091 (2003).

[34] G. Boffetta and R. E. Ecke, *Two-Dimensional Turbulence*, Annu. Rev. Fluid Mech. **44**, 427 (2012).

[35] P. Clark di Leoni and P. D. Minnini, *Quantifying Resonant and Near-Resonant Interactions in Rotating Turbulence*, arXiv:1605.08818.

[36] B. Gallet, *Exact Two-Dimensionalization of Rapidly Rotating Large-Reynolds-Number Flows*, J. Fluid Mech. **783**, 412 (2015).

[37] E. Yarom and E. Sharon, *Experimental Observation of Steady Inertial Wave Turbulence in Deep Rotating Flows*, Nat. Phys. **10**, 510 (2014).

[38] P. Clark di Leoni, P. J. Cobelli, P. D. Mininni, P. Dmitruk, and W. H. Matthaeus, *Quantification of the Strength of Inertial Waves in a Rotating Turbulent Flow*, Phys. Fluids **26**, 035106 (2014).

[39] F. Toschi and E. Bodenschatz, *Lagrangian Properties of Particles in Turbulence*, Annu. Rev. Fluid Mech. **41**, 375 (2009).

[40] T. Elperin, N. Kleeorin, and I. Rogachevskii, *Effect of Chemical Reactions and Phase Transitions on Turbulent Transport of Particles and Gases*, Phys. Rev. Lett. **81**, 2898 (1998).

[41] C. Cambon, F. S. Godeferd, F. C. G. A. Nicolleau, and J. C. Vassilicos, *Turbulent Diffusion in Rapidly Rotating Flows with and without Stable Stratification*, J. Fluid Mech. **499**, 231 (2004).

[42] L. Del Castello and H. J. H. Clercx, *Lagrangian Acceleration of Passive Tracers in Statistically Steady Rotating Turbulence*, Phys. Rev. Lett. **107**, 214502 (2011).

[43] O. Zeman, *A Note on the Spectra and Decay of Rotating Homogeneous Turbulence*, Phys. Fluids **6**, 3221 (1994).

[44] A. Delache, C. Cambon, and F. Godeferd, *Scale by Scale Anisotropy in Freely Decaying Rotating Turbulence*, Phys. Fluids **26**, 025104 (2014).

[45] M. R. Maxey and J. J. Riley, *Equation of Motion of a Small Rigid Sphere in a Nonuniform Flow*, Phys. Fluids **26**, 883 (1983).

[46] M. A. T. van Hinsberg, J. H. M. Thije Boonkkamp, F. Toschi, and H. J. H. Clercx, *On the Efficiency and Accuracy of Interpolation Methods for Spectral Codes*, SIAM J. Sci. Comput. **34**, B479 (2012).

[47] V. Dallas and S. Tobias, *Forcing-Dependent Dynamics and Emergence of Helicity in Rotating Turbulence*, J. Fluid Mech. **798**, 682 (2016).

[48] E. Deusebio, G. Boffetta, E. Lindborg, and S. Musacchio, *Dimensional Transition in Rotating Turbulence*, Phys. Rev. E **90**, 023005 (2014).

[49] B. L. Sawford, *Reynolds Number Effects in Lagrangian Stochastic Models of Turbulent Dispersion*, Phys. Fluids A **3**, 1577 (1991).

[50] S. B. Pope, *Turbulent Flows* (Cambridge University Press, Cambridge, 2000).

[51] L. Smith, J. Chasnov, and F. Waleffe, *Crossover from Two- to Three-Dimensional Turbulence*, Phys. Rev. Lett. **77**, 2467 (1996).

[52] P. Embid and A. Majda, *Low Froude Number Limiting Dynamics for Stably Stratified Flow with Small or Finite Rossby Numbers*, Geophys. Astrophys. Fluid Dyn. **87**, 1 (1998).

[53] L. Bourouiba and P. Bartello, *The Intermediate Rossby Number Range and 2D-3D Transfers in Rotating Decaying Homogeneous Turbulence*, J. Fluid Mech. **587**, 139 (2007).

[54] P. Mininni and A. Pouquet, *Helicity Cascades in Rotating Turbulence*, Phys. Rev. E **79**, 026304 (2009).

[55] P. Bartello, O. Metais, and M. Lesieur, *Coherent Structures in Rotating Three-Dimensional Turbulence*, J. Fluid Mech. **273**, 1 (1994).

[56] J. T. Stuart, *On Finite Amplitude Oscillations in Laminar Mixing Layers*, J. Fluid Mech. **29**, 417 (1967).

[57] F. S. Godeferd, C. Cambon, and S. Leblanc, *Zonal Approach to Centrifugal, Elliptic and Hyperbolic Instabilities in Stuart Vortices with External Rotation*, J. Fluid Mech. **449**, 1 (2001).

[58] J.-N. Gence and C. Frick, *Birth of the Triple Correlations of Vorticity in an Homogeneous Turbulence Submitted to a Solid Body Rotation*, C.R. Acad. Sci., Ser. IIb **329**, 351 (2001).

[59] A. Naso, *Cyclone-Anticyclone Asymmetry and Alignment Statistics in Homogeneous Rotating Turbulence*, Phys. Fluids **27**, 035108 (2015).

[60] H. Aref, *Stability of Relative Equilibria of Three Vortices*, Phys. Fluids **21**, 094101 (2009).
[61] A. Mahalov and Y. Zhou, *Analytical and Phenomenological Studies of Rotating Turbulence*, Phys. Fluids **8**, 2138 (1996).
[62] S. Chakraborty and J. K. Bhattacharjee, *Third-Order Structure Function for Rotating Three-Dimensional Homogeneous Turbulent Flow*, Phys. Rev. E **76**, 036304 (2007).
[63] Y. Zhou, *A Phenomenological Treatment of Rotating Turbulence*, Phys. Fluids **7**, 2092 (1995).
[64] P. D. Mininni, D. Rosenberg, and A. Pouquet, *Isotropization at Small Scales of Rotating Helically Driven Turbulence*, J. Fluid Mech. **699**, 263 (2012).
[65] W.-C. Müller and M. Thiele, *Scaling and Energy Transfer in Rotating Turbulence*, Europhys. Lett. **77**, 34003 (2007).
[66] A. Pouquet and P. D. Mininni, *The Interplay between Helicity and Rotation in Turbulence: Implications for Scaling Laws and Small-Scale Dynamics*, Phil. Trans. R. Soc. A **368**, 1635 (2010).
[67] L. Biferale and I. Procaccia, *Anisotropy in Turbulent Flows and in Turbulent Transport*, Phys. Rep. **414**, 43 (2005).
[68] L. Biferale, D. Lohse, I. M. Mazzitelli, and F. Toschi, *Probing Structures in Channel Flow through SO(3) and SO(2) Decomposition*, J. Fluid Mech. **452**, 39 (2002).
[69] J. Seiwert, C. Morize, and F. Moisy, *On the Decrease of Intermittency in Decaying Rotating Turbulence*, Phys. Fluids **20**, 071702 (2008).
[70] P. D. Mininni, A. Alexakis, and A. Pouquet, *Scale Interactions and Scaling Laws in Rotating Flows at Moderate Rossby Numbers and Large Reynolds Numbers*, Phys. Fluids **21**, 015108 (2009).
[71] M. R. Maxey, *The Gravitational Settling of Aerosol Particles in Homogeneous Turbulence and Random Flow Fields*, J. Fluid Mech. **174**, 441 (1987).
[72] L. Bourouiba, *Discreteness and Resolution Effects in Rapidly Rotating Turbulence*, Phys. Rev. E **78**, 056309 (2008).
[73] L. M. Smith and Y. Lee, *On Near Resonances and Symmetry Breaking in Forced Rotating Flows at Moderate Rossby Number*, J. Fluid Mech. **535**, 111 (2005).